Aerosol Science & Technology

ISSN: 0278-6826 (Print) 1521-7388 (Online) Journal homepage: https://www.tandfonline.com/loi/uast20

Experimental Study of Particle Losses Close to the Entry of Thin-Walled Sampling Probes at Varying Angles to the Wind

Avula Sreenath , Gurumurthy Ramachandran & James H. Vincent

To cite this article: Avula Sreenath , Gurumurthy Ramachandran & James H. Vincent (2001) Experimental Study of Particle Losses Close to the Entry of Thin-Walled Sampling Probes at Varying Angles to the Wind, Aerosol Science & Technology, 35:3, 767-778, DOI: 10.1080/02786820152546815

To link to this article: https://doi.org/10.1080/02786820152546815

Aerosol Science and Technology 35: 767–778 (2001)

Published by Taylor and Francis
0278-6826/01/$12.00 + .00

Experimental Study of Particle Losses Close to the Entry of Thin-Walled Sampling Probes at Varying Angles to the Wind

Avula Sreenath,[1] Gurumurthy Ramachandran,[2] and James H. Vincent[3]

[1]*TSI Incorporated, Shoreview, Minnesota*
[2]*Division of Environmental and Occupational Health, School of Public Health, University of Minnesota, Minneapolis, Minnesota*
[3]*Department of Environmental Health Sciences, School of Public Health, University of Michigan, Ann Arbor, Michigan*

This article summarizes the results of an extensive experimental study of sampling losses in thin-walled probes at various values of velocity ratio *R* and the probe orientation with respect to the freestream. The purpose of this study was to gain insights into the complex interaction of various parameters that influence sampling losses and the consequent effect on the overall sampling efficiency. A 0.635 cm diameter sharp-edged tube was mounted in a small wind tunnel where the freestream velocity could be varied over a wide range of values. Polydispersed spherical glass beads were used as the test aerosol. The number concentration and the particle size distribution were measured using the aerodynamic particle sizer (APS 3310). The sampling efficiency was determined as a function of orientation for a range of particle sizes (or Stokes number). By using an existing model to predict the aspiration efficiency for thin-walled probes, the sampling losses could be isolated from the sampling efficiency. In this manner a new empirical model was developed to predict the losses as a complex function of Stokes number, sampler orientation, and velocity ratio. The losses appear to be influenced by particle inertia, impaction, gravitational settling in the boundary layer developing inside the thin-walled probe, and *vena contracta* or flow recirculation loss near the entry. It was evident from the results that these losses are strongly influenced by the Stokes number and sampler orientation. The losses also increased strongly with increasing value of velocity ratio for all orientations.

INTRODUCTION

The cylindrical thin-walled probe is one of the most extensively studied of all aerosol samplers (as reviewed by Vincent 1989, 1995). It is the most idealized form of aerosol sampler, and one that is most amenable to study and develop theoretically. It also has important applications in its own right, especially in the area of stack sampling for determining particulate emissions from industrial plants. Further, the knowledge gained from understanding the performance characteristics of thin-walled probes has been applied to the understanding of much more complex sampling systems such as those used in environmental and occupational hygiene.

For the thin-walled probe, most of the research since the 1960s has focused on tubes either facing into the freestream or at relatively small angles to it (e.g., Belyaev and Levin 1974; Durham and Lundgren 1980; Jayasekara and Davies 1980; Davies and Subari 1982; Tufto and Willeke 1982a,b; Vincent et al. 1986; Okazaki et al. 1987a,b,c; Okazaki and Willeke 1987; Wiener, Okazaki, and Willeke 1988; Hangal and Willeke 1990; Grinshpun et al. 1993; and many others). But experimental data by which to characterize performance at large angles to the freestream are sparse.

Aspiration is the physical process of drawing in an aerosol from an environment and past the plane tangential to the sampler orifice. For a tube sampling aerosols uniformly distributed in a uniform freestream, aspiration efficiency (A) may be defined as the ratio of the concentration entering through the plane of the entry of the tube (c_1) to that in the undisturbed upstream air (c_0) (Vincent 1989). It depends on the Stokes number, St, the ratio of the freestream velocity (U) to the sampling velocity at the tube entrance (U_s), $R(= U/U_s)$, and the orientation of the sampler to the freestream (α). Here, $St = d_{ae}^2 \gamma^* U/18\eta D$ embodies the effects of particle inertia, in which d_{ae} is the particle aerodynamic diameter, D the width of the sampling inlet, γ^* the density of water (10^3 kg/m^3), and η the viscosity of air.

Although A is the most basic index of performance for the sampler, the actual performance in practice is complicated by

Received 22 February 2000; accepted 13 July 2000.
This work was carried out under CDC-NIOSH contract 5 RO1OH02984-03. The authors are grateful for this support.
Address correspondence to Gurumurthy Ramachandran, Division of Environmental and Occupational Health, School of Public Health, University of Minnesota, Box 807 Mayo, 420 Delaware Street S.E., Minneapolis, MN 55455. E-mail: ram@cccs.umn.edu

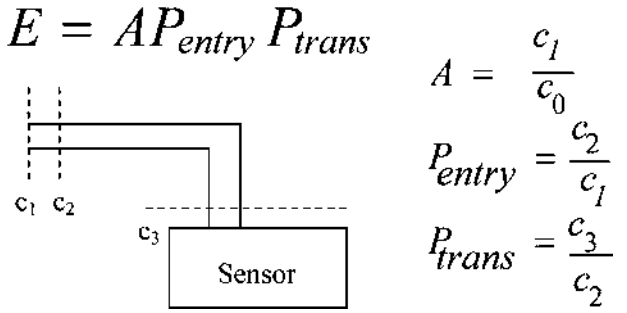

Figure 1. Definitions of aspiration efficiency (A), entry penetration (P_{entry}), tube penetration (P_{trans}), and sampling efficiency (E).

the fact that the aspirated aerosol has to adjust to the new flow conditions inside the tube. This in turn means that there will be particle losses in the so-called "entry region" (within a few diameter lengths past the entry plane) directly as a result of this transition or "coupling" between the external and internal flows. In addition, beyond the entry region, the aerosol must pass through a length of tube before it reaches the sensing or collecting zone. Thus, there are three distinct regions that need to be discussed when it comes to thinking about overall sampling performance. In general, there are changes in aerosol concentration at all three stages of this process and these result in a measured concentration which is different from the actual concentration in the undisturbed freestream. This difference can be defined in terms of sampling efficiency which, in turn, is a product of three terms (see Figure 1), thus

$$E = AP_{entry}P_{trans} \quad [1]$$

where, E is the overall sampling efficiency. In this relation, A is the aspiration efficiency ($A = \frac{c_1}{c_0}$), P_{entry} is the entry penetration efficiency given by the ratio of particle concentration downstream beyond the entry region of the inlet to that in the plane of the entry ($P_{entry} = \frac{c_2}{c_1}$), and P_{trans} is the ratio of particle concentration at the collection or sensing medium to that just downstream of the entry region ($P_{trans} = \frac{c_3}{c_2}$).

For thin-walled probes, as already stated, aspiration efficiency has been well-characterized and modeled, so too have transmission losses for particle transport through straight and curved tubes. However, very few studies have looked specifically at losses inside the tube close to the entry, with the exception of the work by Hangal and Willeke (1990). Yet this can have a very significant affect on overall sampling efficiency. With this in mind, new experiments were performed to characterize this contribution to sampler performance. Particularly, the effect of orientation on P_{entry} was studied.

PREVIOUS RESEARCH

The importance of internal entry loss was first noted in the early reports of Durham and Lundgren (1980) and Jayasekara and Davis (1980), where it was noted that a large fraction of the aspirated aerosol was deposited on the inner wall of the inlet. But the only data currently available for quantifying internal entry loss comes from the body of work carried out by Willeke and his co-workers to determine the sampling efficiency of thin-walled probes oriented at angles up to 90° from the freestream (Tufto and Willeke 1982a,b; Okazaki et al. 1987a,b,c; Wiener et al. 1988; Grinshpun et al. 1993). They reported that most of the loss occurs within 3 to 5 diameters downstream of the inlet where the flow is very complex, most notably associated with the formation of the *vena contracta* region of separated flow region (including flow reversal) whose structure or properties are poorly understood. They argued that contributions to internal entry loss for tubes oriented at an angle to the freestream come from a combination of gravitational settling, impaction onto inner walls, inward and outward bounce and blow-off, and the losses due to the presence of the *vena contracta*.

For the sampler facing the wind ($\alpha = 0°$), an inlet deposition parameter, K, was identified by Okazaki and Willeke as (1987):

$$K = \sqrt{\frac{Z \cdot St}{\sqrt{Re}}} \text{ or } K = St\sqrt{\frac{g \cdot L \cdot R}{U^2 \cdot \sqrt{Re}}} \quad [2]$$

where Z is the gravitational deposition parameter, g is the acceleration due to gravity, Re is the Reynolds number for the air flow inside the tube, and L is the length of the tube. The parameter K reflects the roles of (1) inertia in decelerating the particles as they enter the tube from the external flow and encounter the more slowly moving air in the boundary layer inside the tube, and (2) gravity in bringing about deposition. From their experimental data, Willeke and his colleagues developed the empirical relation

$$P_{entry} = \exp(-4.7\ K^{0.75}) \quad [3]$$

for $\alpha = 0°$ in the vertical plane. The same group later went on to study what happened for a tube oriented at angles greater than facing the wind, with $\alpha = 15°, 30°, 60°$, and 90°. Now the inlet deposition parameter was modified to the form

$$K_\alpha = \sqrt{\frac{St \cdot Z \cdot \cos(\alpha)}{\sqrt{Re}}} = K(\cos(\alpha))^{0.5} \quad [4]$$

Furthermore, it was assumed that the entry efficiency, P_{entry}, is a product of two components, the gravitational part (E_s) and the impaction part (E_i), so that

$$P_{entry} = E_s \cdot E_i \quad [5]$$

where the impaction losses are also dependent on the orientation of the sampling probe. Here the losses occur due to (1) particle impaction on to the portion of the inside wall of the tube exposed directly to the upstream flow, and (2) particle deflection by the *vena contracta* near the inlet. For the first of these,

particle motion toward the wall is influenced by $U \cdot \sin(\alpha)$ and $v_s \cdot \cos(\alpha)$, where v_s is particle settling velocity. When the sampler is upward facing, the velocity components are additive and, when the sampler is downward-facing, the components oppose each other. By considering a limiting particle trajectory beyond which a particle will get deposited, an impaction region can be estimated by calculating the stopping distance which is a function of $U \cdot \sin(\alpha)$ and v_s. The depth of this region depends on whether the gravity enhances impaction when sampling upward or reduces impaction while sampling downward. For sampling upward, gravitational settling and freestream velocity act together, while for sampling downward they act against each other. The effect of gravity may then be expressed as determined by Hangal and Willeke (1990):

$$I_w = St \cdot (R)^{0.5} \cdot \sin(\alpha \pm \gamma) \cdot \sin\left(\frac{(\alpha \pm \gamma)}{2}\right) \qquad [6]$$

where I_w is loss due to impaction on to the inner walls of the thin-walled tube, and γ is referred to as the "gravity angle"—the incremental angle that produces an effect equivalent to the impaction loss caused by gravity which is either added or subtracted from the sampling inlet angle.

The presence of the *vena contracta* region causes flow disturbances due to changes in pressure distribution, which increases particle deposition. For the thin-walled tube, the critical bits of information are the amount of entrained flow in the *vena contracta* and the removal efficiency of particles entering the *vena contracta*. From such considerations, Hangal and Willeke (1990) (I_v) expressed losses due to the *vena contracta* as

$$I_v = 0.09\left(\left[\frac{1-R}{R}\right] \cdot St \cdot \cos(\alpha)\right)^{0.3} \qquad [7]$$

where it was assumed that I_v goes to zero when $R > 1$, based on the assumption that the *vena contracta* is not formed when $R > 1$. Equation (7) was based on the theory that *vena contracta* losses were assumed to be proportional to the amount of entrained flow in to the *vena contracta* and the particle stopping distance. They then wrote down the total entry efficiency due to both impaction and the *vena contracta* effect in the form

$$E_i = \exp(-75(I_w + I_v)^2) \qquad [8]$$

Ideas like those contained in the work described above provide the starting point for the present article.

EXPERIMENTAL

Apparatus

The experimental facilities and methods used in this research have been described in detail elsewhere (Ramachandran, Sreenath, and Vincent 1998), so only a short summary will be given here. The experiments were conducted in a small open-loop wind tunnel (Figure 2a). Well-defined turbulence in the working section was generated using a lattice-type screen placed at the entrance to the working section, with intensity and length scale estimated at about 5% and 0.7 cm respectively for all of the experiments described. Test aerosol was generated using polydisperse glass microbead powders (Cataphote Inc., Jackson, MS), aerosolized by means of a powder disperser (Model NBS-II, BGI Inc., Waltham, MA) with a venturi-type aspirator. In this way, aerosol was generated with particles in the range of aerodynamic diameters between 1 and 37 μm. Before injection into the wind tunnel, it was passed through a 2 mCi Kr^{85} neutralizer (Model 3012, TSI Inc., St. Paul, MN), and then through a 90° bend into a 0.76 cm diameter injection nozzle. A mixing plate of area equal to half that of the duct was placed immediately downstream of the injection point inside the wind tunnel to help disperse the aerosol efficiently. In preparation for the experiments, the glass beads were stored in a heated oven to reduce the

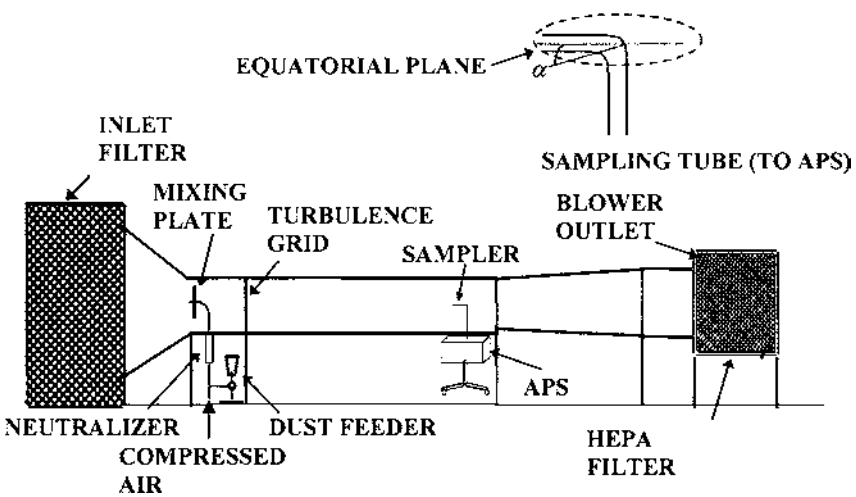

Figure 2a. Schematic diagram of experimental apparatus.

moisture content and then sieved to remove any large agglomerates before placement in the powder disperser. An infrared lamp was used to maintain the heat in the dust in the disperser in order to reduce subsequent moisture adsorption, agglomeration and clogging of the dust hopper. By these means, a highly constant, agglomerate-free aerosol output (number concentrations constant to within $\pm 1\%$) was achieved for up to 3 hours.

For the experiments reported in this article, we employed a thin-walled sampling probe of diameter $D = 0.635$ cm in the sampler configuration shown in Figure 2a, where the 90° elbow downstream of the inlet is evident. The sampled aerosol entered the sampler through this tube, which was connected directly to an aerodynamic particle sizer (APS; Model 3310, TSI Inc., St. Paul, MN). By this direct-reading instrument, the sampled particles were measured and counted into bins representing particle size intervals between 0.5 and 30 μm (with the data stored in a personal computer that also controlled the APS operation). The overall sampling system was arranged in such a way that the orientation of the tube entry with respect to the freestream (α) could be varied from 0° to 180° in the horizontal plane, quite different from the studies by Willeke and his colleagues (Hangal and Willeke 1990), where the sampling tube was rotated up or down in the vertical plane. This ensured that losses associated with particle deposition due to gravitational and other forces along the majority of the length of the tube remained unchanged as α was varied. The sampling flowrate for all the experiments described was varied from 2 lpm to 20 lpm. Even though the APS itself operates at 5 L/min, an adapter was used to either draw extra flow or supply additional air to the APS when sampling at flow rates other than 5 lpm. A schematic of this adapter is shown in Figure 2b. The dimensions of this adapter were selected to ensure the absence of recirculation flows in the adapter and enable particles to be concentrated at the center of the adapter. This adapter could be snapped on the APS inlet using a quick-connect. For flows other than 5 lpm, two symmetrically opposite ports were connected to a pump through which air was either drawn in or forced out to obtain the desired net sampling flow rate. For example, to obtain a sampling flow of 20 lpm, the APS would draw 5 lpm while the external pump would draw 15 lpm. The free stream velocity in the wind tunnel was kept a constant at 4 m/s. Hence R was changed by changing only the sampling velocity. The aerosol generation rate was adjusted so that the APS provided particle counts for each particle size bin in the range from 10 to 20 particles/cm^3, thus providing good count statistics with minimal coincidence problems.

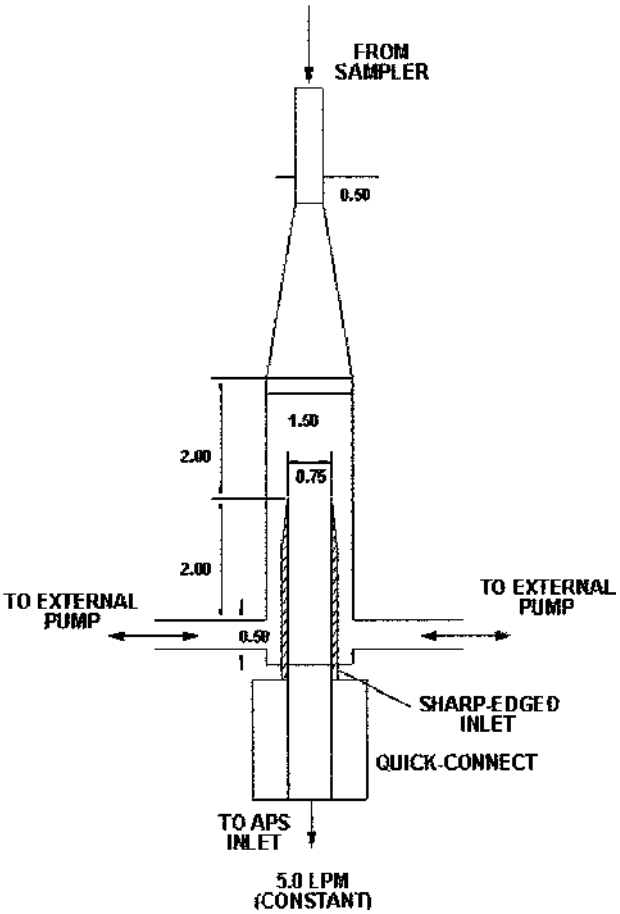

Figure 2b. Schematic of the APS inlet adapter. (All dimensions are in inches.)

Experimental Rationale

In general, aspiration efficiency of a sampling probe at some angle α to the freestream is defined as

$$A_\alpha = \frac{c_\alpha}{c_0} \qquad [9]$$

where c_α is the inlet concentration at angle α, and c_0 is the concentration in the undisturbed freestream. However, the experimental procedures adopted with this apparatus were significantly different from most related experiments cited in the literature. In our experiments, we decided not to measure c_0 directly. Instead, we proceeded as follows, beginning by rewriting Equation (9) in the form

$$A_\alpha = \frac{{}_1c_\alpha}{c_0} = \frac{{}_1c_\alpha}{{}_1c_{(\alpha=0)}} \times \frac{{}_1c_{(\alpha=0)}}{c_0} = \frac{{}_1c_\alpha}{{}_1c_{(\alpha=0)}} \times A_{\alpha=0} \qquad [10]$$

where ${}_1c_\alpha$ is the measured inlet concentration (and the prefix 1 refers to the plane of the sampler inlet and subscript 0 refers to a plane far upstream of the flow where the presence of the sampler is not felt), ${}_1c_{(\alpha=0)}$ is the inlet concentration measured using the sampler facing the freestream, and A_0 is the aspiration efficiency of the sampler for the simplest case when it is facing the freestream. In order to calculate the aspiration efficiency at an angle α, the aspiration efficiency for the sampler facing the wind ($\alpha = 0°$), therefore, also needs to be known. It is fortunate that this can be calculated with considerable confidence from existing theory (e.g., Vincent et al. 1986). Ideally, therefore, a measurement of the ratio ${}_1c_\alpha/{}_1c_{(\alpha=0)}$ can be used along with the theoretically known value of $A_{\alpha=0}$ to determine A_α.

However, in reality, a measurement of ${}_1c_\alpha/{}_1c_{(\alpha=0)}$ cannot be obtained directly unless the sampling efficiency is a constant and is independent of the orientation. In other words, Equation (10) is valid only if the losses in the sampling system are the same when the sampler is facing the freestream and facing away from the freestream. In other words, the losses must remain constant at all angles. Taking all the losses along the whole length of the sampling train into account, we define sampling efficiency as

$$E_\alpha = \frac{{}_{APS}c_\alpha}{c_0} \qquad [11]$$

where ${}_{APS}c_\alpha$ is the particle concentration reaching the APS for the orientation indicated. Since c_0 cannot be determined directly in our experimental system, what is actually measured is the sampling efficiency ratio (H_α) given by

$$H_\alpha = \frac{{}_{APS}c_\alpha}{{}_{APS}c_{\alpha=0}} = \frac{E_\alpha}{E_{\alpha=0}} \qquad [12]$$

The sampling efficiency data that will be presented in a later section is a plot of the product of H_α and $E_{\alpha=0}$, which is the true sampling efficiency. The losses in the tube including the bend are given by $(1 - P_{tube})$, where $P_{tube}(= {}_{APS}c_\alpha/{}_2c_\alpha)$ remains constant for any value of α by the virtue of the way the experiments were designed. Here, the prefix 2 refers to a plane just downstream of the inlet. The entry losses between planes 1 and 2 are dependent on the orientation, α while the tube losses between plane 2 and the APS are independent of orientation. This ensures that the tube losses are canceled out while taking a ratio of these two concentrations. H_α and P_{tube} are related by

$$H_\alpha = \frac{{}_2c_\alpha \cdot P_{tube}}{{}_2c_{\alpha=0} \cdot P_{tube}} = \frac{{}_1c_\alpha \cdot P_{entry(\alpha)}}{{}_1c_{\alpha=0} \cdot P_{entry(\alpha=0)}} \qquad [13]$$

where ${}_2c_\alpha$ is the particle concentration inside the sampler where the flow has reached a new equilibrium (that is, it does not remember the external flow). In the above expression, unlike P_{tube} that remains constant for all angles, P_{entry} depends on α. As a consequence, the contributions to entry loss from direct impaction, the *vena contracta* and the boundary layer effects change with orientation. E_α may be further linked with aspiration efficiency by relating ${}_1c_\alpha$ to c_0 through Equation (9). We may relate aspiration efficiency to E_α by

$$H_\alpha = \frac{{}_1c_\alpha \cdot P_{entry(\alpha)}}{{}_1c_{\alpha=0} \cdot P_{entry(\alpha=0)}} = \frac{A_\alpha \cdot c_0 \cdot P_{entry(\alpha)}}{A_{\alpha=0} \cdot c_0 \cdot P_{entry(\alpha=0)}} = \frac{A_\alpha \cdot P_{entry(\alpha)}}{A_{\alpha=0} \cdot P_{entry(\alpha=0)}} \qquad [14]$$

so that

$$A_\alpha \cdot P_{entry(\alpha)} = H_\alpha \cdot A_{\alpha=0} \cdot P_{entry(\alpha=0)} \qquad [15]$$

In the above expression, H_α is what is actually measured in our experiments. The quantities A_α and $A_{\alpha=0}$ may be calculated from the current theory of thin-walled sampling probes for angles up to 90° (e.g., Vincent et al. 1986; Vincent, 1989), and $P_{entry(\alpha=0)}$ may be obtained from the model of Okazaki and Willeke (1987) summarized above. From the literature cited, it is seen that these models reflect very closely what has been measured experimentally. This approach therefore allows us, with confidence, to determine $P_{entry(\alpha)}$. This is the subject of interest in this work.

Experimental Methods

For each measurement of H_α, the number concentration was recorded eleven times: six times at the forward-facing orientation to provide an average value of ${}_{APS}c_{\alpha=0}$, and five times at orientation α to provide an average value of ${}_{APS}c_\alpha$. To ensure that any count differences between the positions were not caused by any temporal shifts in the aerosol generation rate, the concentrations were measured at the two positions in a "*0-α-0-α-0-α-0-α-0-α-0*" sequence. By solving Equation (15) for $P_{entry(\alpha)}$ the following relationship was developed.

$$P_{entry(\alpha)} = H_\alpha \cdot \frac{A_{\alpha=0} \cdot P_{entry(\alpha=0)}}{A_\alpha} \qquad [16]$$

The experiments were performed for α-values in the horizontal plane ranging from 0° to 90° in steps of 15°, and for a single freestream velocity of 4 m/s. Three sampling flowrate conditions were employed, 2 Lpm, 5 Lpm, and 20 Lpm, corresponding to R values of 3.8, 1.52 and 0.38 respectively. In all the experiments, the outer edge of the thin-walled probe was greased to avoid any particle bounce.

RESULTS

It may be noted once again, that the effects of gravity were constant since the measurements of H_α and $H_{\alpha=0}$ were made on the same sampling plane. Therefore, for a fixed freestream velocity and sampling flow rate (i.e., fixed R), the aspiration efficiency and the entry losses may be regarded as influenced by just three independent dimensionless parameters: α, R, and St. The effects of these on $P_{entry}(\alpha)$ are therefore elaborated in the experimental results presented below by reference to two sets of graphs: $E_\alpha\ (= H_\alpha \cdot A_{\alpha=0} \cdot P_{entry(\alpha=50)})$ versus St for different α for three values of R, and $P_{entry}(\alpha)$ versus St for different α for three values of R. In all these plots, the x-axis is in the logarithmic scale for enhanced clarity. In addition, three-dimensional graphs are also presented to show the overall picture.

Figure 3a shows experimental results for the effect of α on E_α for increasing St and for $R = 1.52$. It is seen that, for all angles and for $St < 0.1$, E_α decreases with increasing St. But as St increases beyond 0.1, E_α reverses its trend and increases for St up to about 0.3, after which it decreases again. Hence, a local minimum is seen around $St = 0.1$, and this does not change much with α. The depth of the minimum increases for angles increasing up to $\alpha = 45°$. Beyond this, the dip decreases with increasing α and eventually disappears at $\alpha = 90°$. Similarly, the increase in E_α for St beyond the local minimum is restricted only

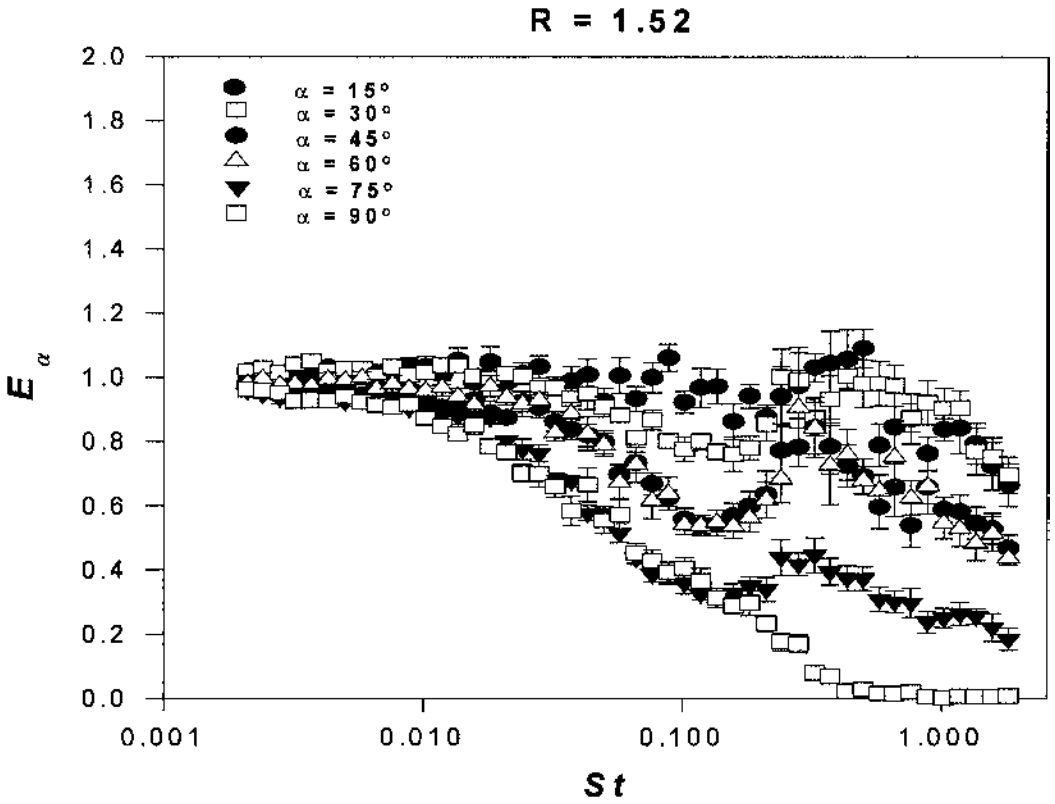

Figure 3a. Sampling efficiency versus *St* for different orientations to the freestream for $R = 1.52$. $E_\alpha = H_\alpha \cdot A_{\alpha=0} \cdot P_{entry}$.

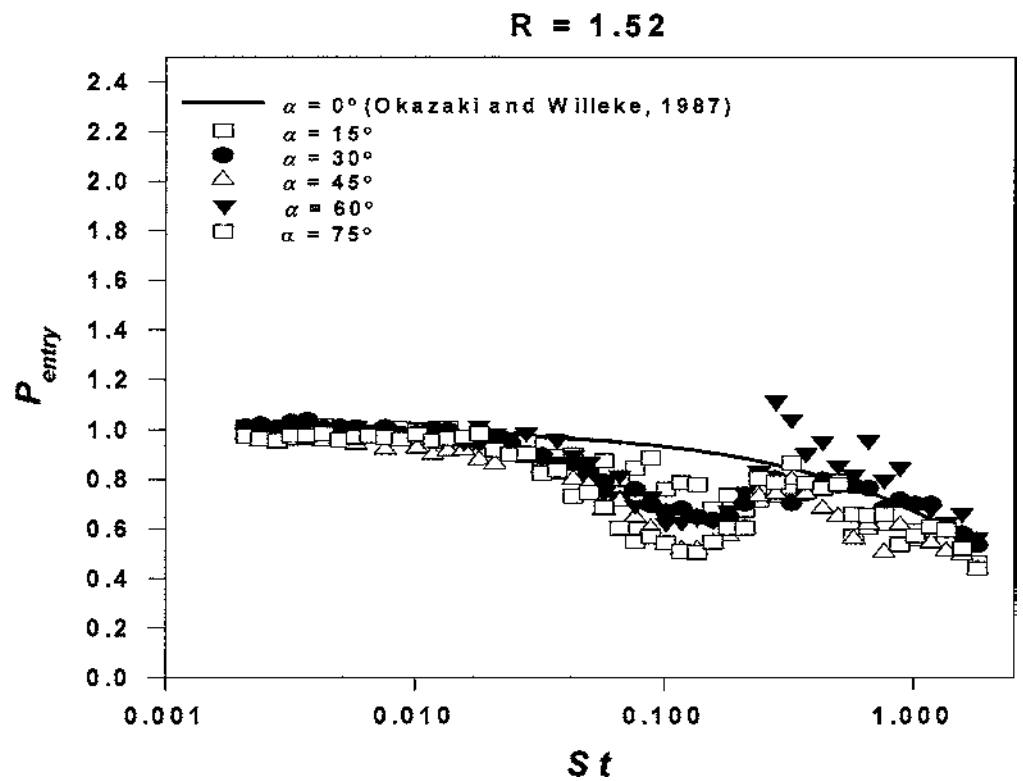

Figure 3b. Entry penetration versus *St* number for different orientations to the freestream for the same value of *R*.

up to about $St = 0.3$, after which it falls again. Thus, the trend of an initial decrease in E_α followed by an increase weakens until the point is reached at about $\alpha = 90^\circ$ where it becomes a monotonically decreasing function of St, reaching zero at about $St = 0.4$. We hypothesize that the formation of a minimum at around $St = 0.1$ is a result of complex interaction between various physical processes that influence particle deposition.

We now proceed to determine $P_{entry}(\alpha)$ for the same set of experimental conditions. For this, we use the well-tested model for aspiration efficiency for thin-walled probes at α to the freestream given by Vincent et al. (1986) and Vincent (1987) as

$$A_\alpha = 1 + \left[1 - \frac{1}{1 + G(\alpha) \cdot St(\cos(\alpha) + 4R^{1/2}(\sin(\alpha))^{0.5}}\right] \times (R \cdot \cos(\alpha) - 1), \quad [17]$$

where G is a fitted coefficient determined by experiments. Here it is seen that, for angles less than 45° and for $R = 1.52$, $R \cdot \cos(\alpha)$ should be greater than 1; conversely, for angles greater than 45°, $R \cdot \cos(\alpha)$ should be less than 1. However, this tendency is not reflected in Figure 3a. So there is a clear discrepancy between aspiration efficiency and the experimental results for most values of α up to 90°. At $\alpha = 90^\circ$, however, the results for sampling efficiency in Figure 3a fall into good agreement with the expected aspiration efficiency. Further, Okazaki et al. (1987a) found that entry losses are significant only up to $\alpha = 60^\circ$ and at $\alpha = 90^\circ$ only aspiration efficiency is a significant contributor to the overall sampling efficiency. These observations strongly suggest that particle losses just inside the sampler inlet are playing a significant role in the discrepancy at smaller angles. But at $\alpha = 90^\circ$ the effect disappears because the inside wall of the sampling tube projects zero area to the upstream flow, thus eliminating the possibility of direct impaction. Also the shape of the *vena contracta* is a lot different from an inlet facing the freestream. Therefore, results for $P_{entry}(\alpha = 90^\circ)$ are not presented in Figure 3b.

With the preceding in mind, Figure 3b is a plot of $P_{entry}(\alpha)$ versus St determined from our experimental results for different values of α, again for $R = 1.52$. Also shown is the curve calculated from the model of Okazaki and Willeke (1987) for $\alpha = 0^\circ$. There is fair agreement between our results plotted in this way and the Okazaki and Willeke model, except that, for angles greater than 0°, a dip appears which becomes deeper with increasing α. Beyond $St \approx 0.04$, $P_{entry}(\alpha)$ falls again with increasing St. From Figure 3b, it is clear that a local maximum and a local minimum are created as St increases. This is true for all α except $\alpha = 90^\circ$ (results for which are not shown in Figure 3b). This suggests that the overall $P_{entry}(\alpha)$ is influenced by two competing mechanisms, each dominant over a certain regime of St and α. The exact nature of this mechanism is not clear, but for the present purpose they can be characterized by fitting empirical expressions.

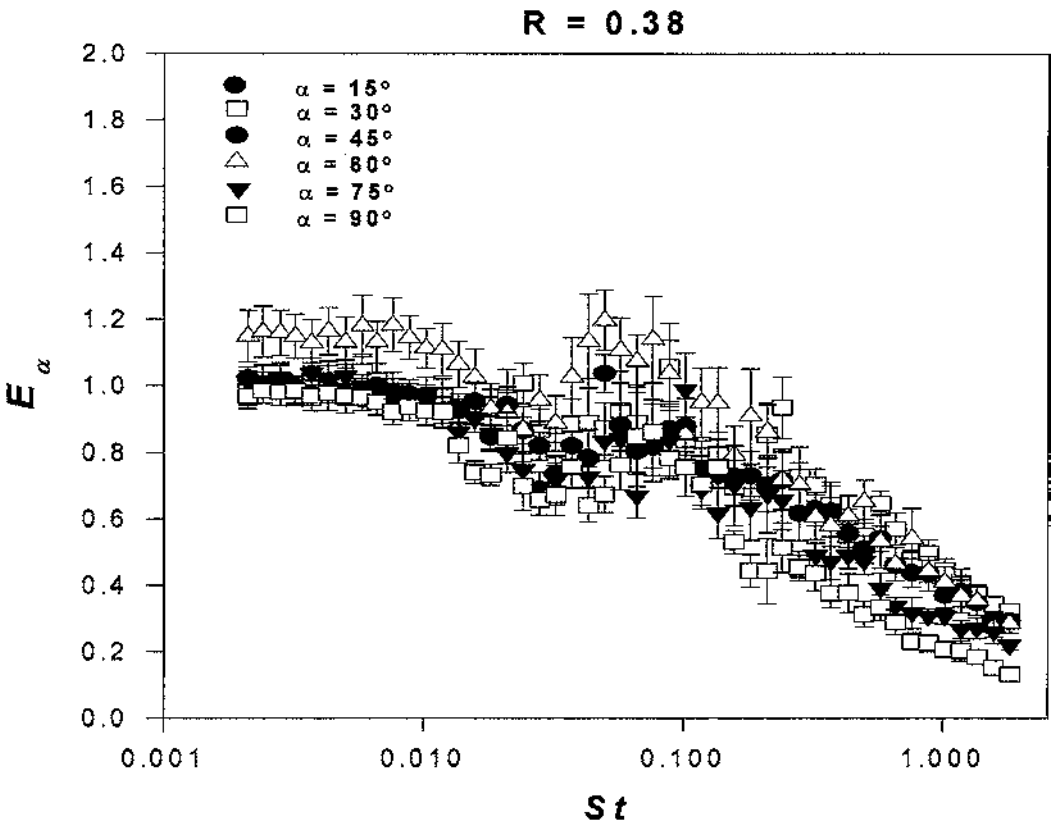

Figure 4a. Sampling efficiency versus St for different orientations to the freestream for $R = 0.38$. $E_\alpha = H_\alpha \cdot A_{\alpha=0} \cdot P_{entry(\alpha=50)}$.

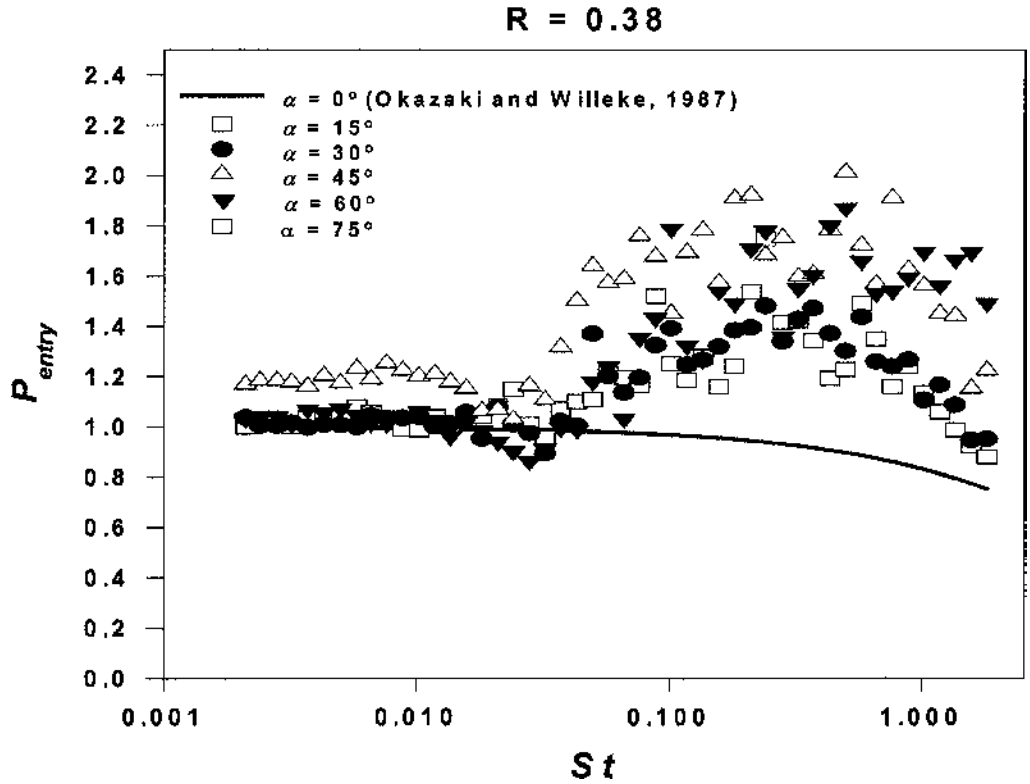

Figure 4b. Entry penetration versus *St* for different orientations to the freestream for the same value of *R*.

Figure 4a shows the effect of *St* and α on E_α for $R = 0.38$, representing a much higher sampling velocity. The trends do not change much for small values of α, but become noticeable for larger values in the range $\alpha = 60^\circ$ to 90°. In general, E_α decreases with increasing *St* until a minimum is reached at about $St = 0.02$, beyond which it rises again briefly. Thereafter it reaches a maximum at about $St = 0.1$, after which it falls again as the *St* is further increased. For all α, the locations of this minimum and maximum do not change much. It is interesting to note that, in contrast to the case of $R = 1.52$, the trend for $\alpha = 90^\circ$ is not monotonic. Therefore, the results are not consistent with what we know about aspiration efficiency. This also indicates that losses are strongly dependent on the sampling velocity. It will be shown later that at very low sampling velocities ($R = 3.8$), the trends are far more predictable.

Figure 4b shows the corresponding results for the effect of *St* and α on $P_{entry}(\alpha)$ for $R = 0.38$. It is evident that the entry losses are negligible at low *St* and continue to drop slightly as *St* increases. But after reaching a small minimum at about $St = 0.02$, $P_{entry}(\alpha)$ actually increases. Of course, the values that are greater than unity might be the result of re-entrainment of particles. This upwards trend continues until about $St = 0.3$, beyond which $P_{entry}(\alpha)$ starts to decrease, even though it remains above unity. It should be noted, however, that the results exhibit considerable scatter in this region.

Figure 5a describes the effect of α on E_α for increasing *St* for $R = 3.8$, and here the sampling velocity was the lowest of all three cases studied. Comparing with the earlier Figures 3a and 4a, it is seen that the trends are significantly different from those for $R = 0.38$ but similar to those observed for $R = 1.52$. However, the location of the minimum is now shifted to about $St = 0.2$ and the corresponding maximum is almost nonexistent. The corresponding results for the effects of *St* and α on $P_{entry}(\alpha)$ are shown in Figure 5b. Now the penetration efficiency is markedly less than that predicted for $\alpha = 0^\circ$ using the model of Okazaki and Willeke (1987). Similar to the case where $R = 1.52$, there is no significant influence of α on $P_{entry}(\alpha)$.

DISCUSSION

Modeling $P_{entry}(\alpha)$

From the earlier discussion on losses in thin-walled probes, it is evident that the entry losses should include gravitational settling, losses due to direct impaction on to the inner walls of the probe and also entrainment of particles into the *vena contracta* recirculating flow region that is formed inside the sampling nozzle. Although the shape and size of the *vena contracta* is unknown, let us assume that a portion of particles N_1 entering the nozzle are entrapped in the *vena contracta* (N_2). Some fraction κ of the particles in the *vena contracta* are lost by inertial deposition on the nearby wall, so that the number of particles lost to the walls is κN_2. Then the number of particles available for direct impaction and gravitational settling is $(N_1 - \kappa N_2)$.

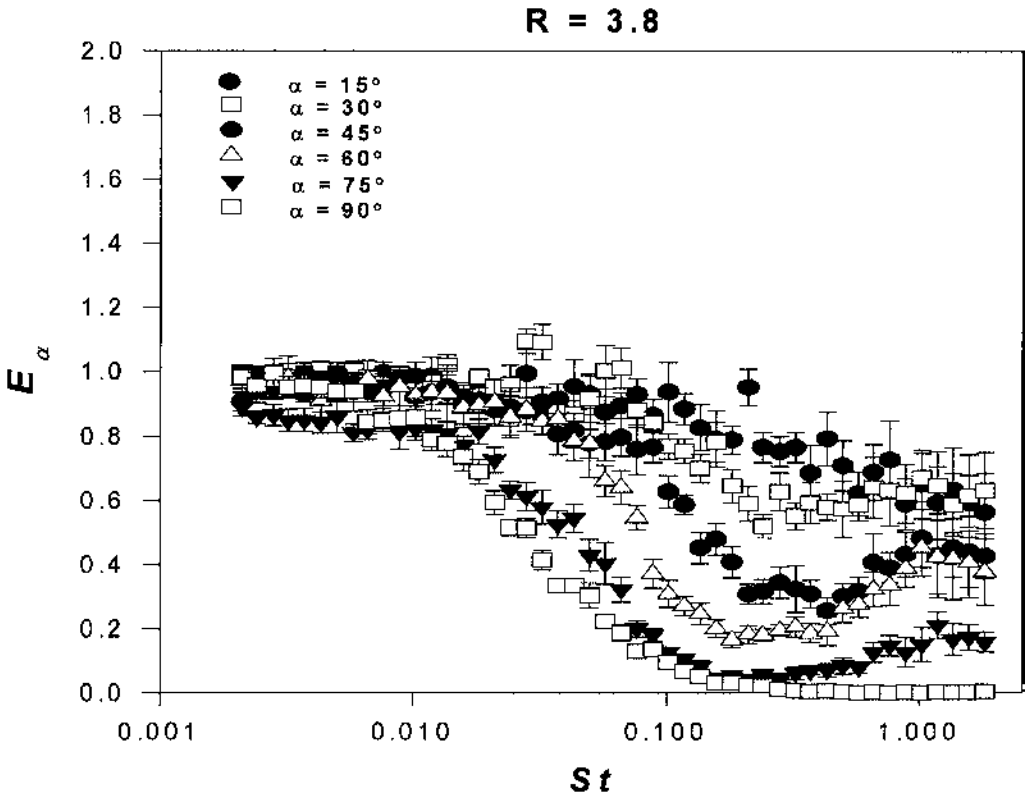

Figure 5a. Sampling efficiency versus *St* for different orientations to the freestream for $R = 3.8$.

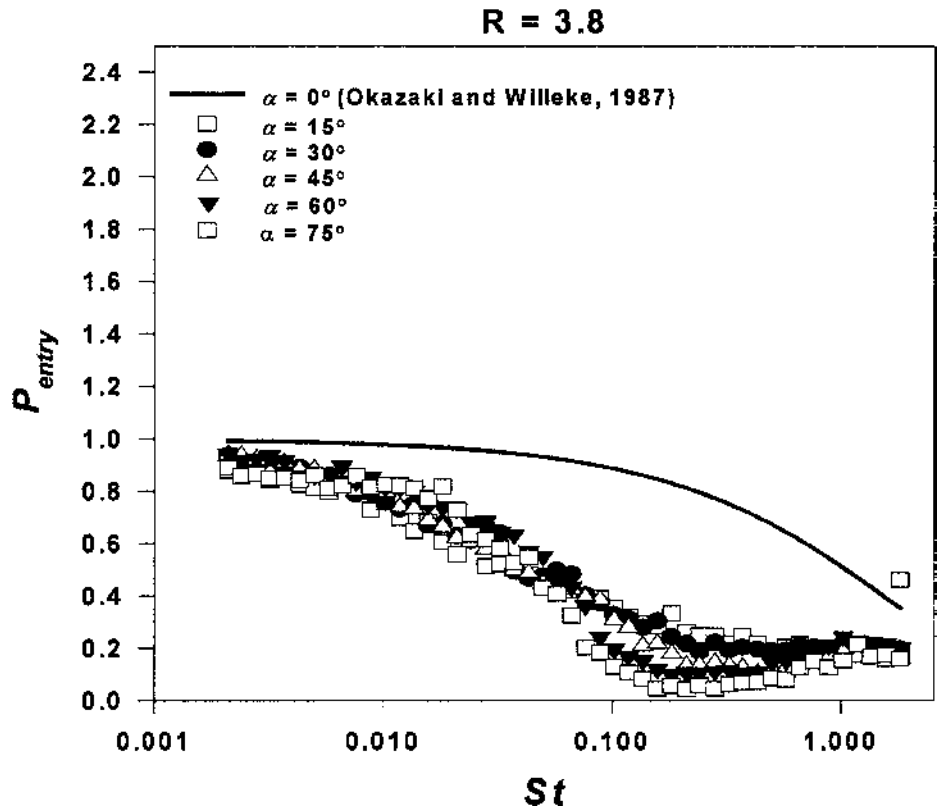

Figure 5b. Entry penetration versus *St* for different orientations to the freestream for the same value of *R*.

If ε is the efficiency of the initial direct impaction and G is the efficiency of deposition due to the effect of gravity, then the number of particles N_3 that penetrate the entry after taking into account losses due to impaction and gravity to the wall will be given by

$$N_3 = (N_1 - \kappa N_2)(1 - \varepsilon)(1 - G). \quad [18]$$

The above expression can then be reduced to

$$N_3 = N_1\left(1 - \kappa\frac{N_2}{N_1}\right)(1 - \varepsilon)(1 - G). \quad [19]$$

The entry penetration efficiency is therefore given by

$$\frac{N_3}{N_1} = P_{entry} = \left(1 - \kappa\frac{N_2}{N_1}\right)(1 - \varepsilon)(1 - G). \quad [20]$$

In this expression, the first term describes particle collection by entrainment into and inertial deposition from the *vena contracta* and collection by impaction onto the walls, the second term describes collection by direct impaction of the particles onto internal surfaces "exposed" to the freestream, and the third term describes particle collection due to gravitational settling. Since the first and second terms are dependent on particle inertia, they each may be jointly expressed in the general form $\{1 - f(St, R, \alpha)\}$. The third term can be expressed as a modified form of Hangal and Willeke's (1990) expression for P_{entry} for $\alpha = 0^\circ$. Any empirical model should comply with the following boundary conditions:

1. For $St \to 0$, $P_{entry}(\alpha) \to 1$ for all α.
2. For $\alpha \to 0$, $P_{entry}(\alpha) \to \exp(-4.7K^{0.75})$ from Equation (3)

All the data up to and including $\alpha = 75^\circ$ were considered in this analysis, and were used to obtain a general expression for $P_{entry}(\alpha)$.

The expression that was found for $P_{entry}(\alpha)$ is given by

$$P_{entry}(\alpha) = [1 - c_1 R^{c_2} St^{c_3}(1 - \exp(-c_4\alpha)] \cdot \left(\exp\left(-c_5 \cdot K_\alpha^{c_6}\right)\right) \quad [21]$$

where $c_1, c_2, \ldots c_6$ are empirical coefficients and $K_\alpha = 0.152St\{\cos\alpha/U_s^{2.5}R\}^{1/2}$. Non-linear regression of Equation (21) against the experimental data yields: $c_1 = 0.094$; $c_2 = 1.799$; $c_3 = 0.280$; $c_4 = 142.78$; $c_5 = 71.84$; $c_6 = 1.695$. The corrected-R^2 for this model is 0.65. This form of the equation reduces to Hangal and Willeke's (1990) expression—see Equation (3)—when $\alpha = 0^\circ$.

Three-dimensional plots of model predictions of P_{entry} as a function of α and St are plotted in Figures 6(a), (b), and (c) for the various values of R.

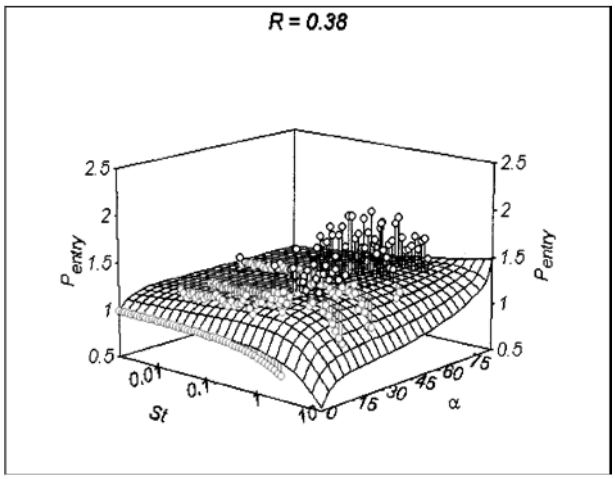

(a)

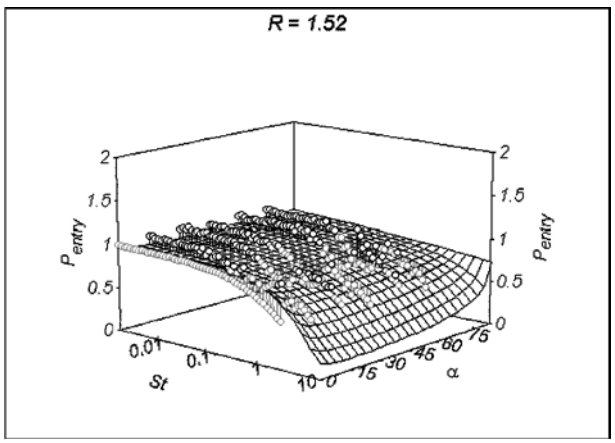

(b)

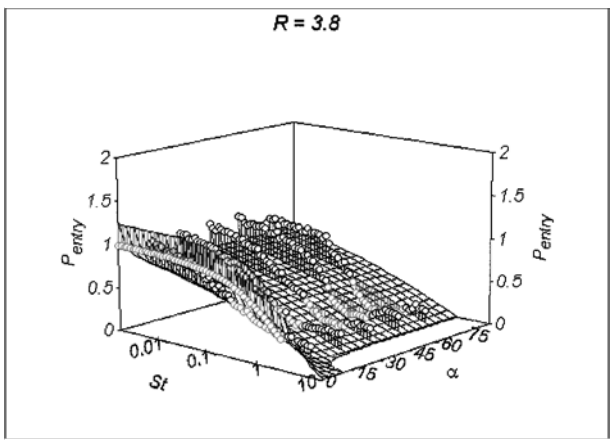

(c)

Figure 6. Model predictions of entry penetration as a function of St and α for: (a) $R = 0.38$; (b) $R = 1.52$; and (c) $R = 3.8$. In all these graphs, the individual data points represent deviations of the measured P_{entry} from model predictions.

Interpretation

The complex patterns shown by the experimental data shown in Figures 3, 4 and 5, in particular the non-monotoni c trends, suggest that the efficiency by which particles are transmitted through

the region just inside the sampling tube is a function of more than one mechanism acting in competition with one another. An empirical model has been developed that invokes three such mechanism—direct impaction, gravitational settling, and inertial deposition from particles entering the *vena contracta* flow region. The empirical model is founded upon physical ideas, but requires the fitting of a number of coefficients. So, although the physical explanation itself is plausible, the quantitative model needs to be treated with caution. On the other hand, the flow inside an aspirating tube placed at an angle to a freestream has never been studied experimentally, numerically, or theoretically. Therefore, there is no previous knowledge on which to base a more concrete model. For the present, therefore, the model that has been described must serve as guidance in the interpretation of what happens not only in the idealized system described here, but also in practical aerosol sampling systems like those used in environmental and occupational hygiene situations.

Figure 6, shows how the predictive model we have developed for P_{entry} compares with the experimental data as a function of both St and α for R ranging from as low as 0.38 to as high as 3.8. Here we see that the model reflects quite well the broad trends determined experimentally. However, there are still some detailed features in the functional relationship that are not explained by the model as presented, including the appearance of dips under certain conditions. This behavior is a function of the extreme complexity of the three-dimensional, asymmetric fluid, and particle motions in the region near the sampling inlet, and is a reminder that the model remains just a fair approximation deserving further explanation. Nonetheless, in the meantime, the model as it stands will be very helpful in understanding the performances of thin-walled sampling probes in practical situations. It will also provide insights toward the performance characteristics of other, more complicated sampling systems.

The *vena contracta* contribution itself is very complex and merits further discussion, albeit qualitative. We may consider that some small particles may readily diffuse into the *vena contracta* region, but then, because of the weak inertial forces, may diffuse back into the main flow. So, to outward appearances, they remain essentially unaffected by the *vena contracta*. Much larger particles will have sufficient inertia that they will be unaffected by the flow distortion represented by the *vena contracta* flow, and so will pass straight on. It is, of course, likely that they may be collected in the entry region by direct impaction and gravitational deposition. As a consequence, at large St, the sampling efficiency decreases rapidly irrespective of R or α. Between these two extremes, however, there will be an intermediate range of conditions within which particles may enter the *vena contracta* flow region by virtue of their inertia but, once entrained in this way, will exhibit sufficient inertia inside that recirculating flow region to migrate to the wall there and be collected. It is in this size range that it is plausible for the entry loss to increase (and hence penetration to decrease), as we observed in the forms of the minima exhibited by our experimental data. The phenomenon we have described is somewhat

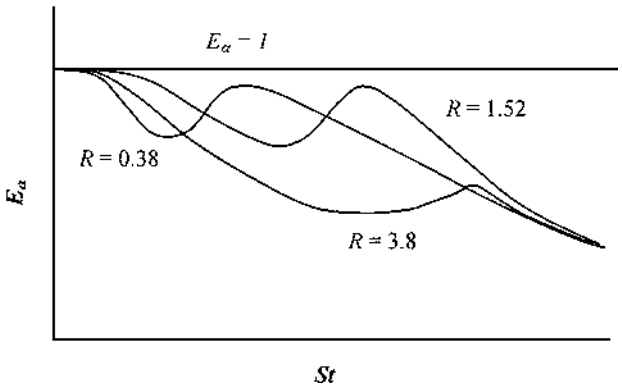

Figure 7. Schematic diagram illustrating the effect of R on the sampling efficiency at an arbitrary orientation (α).

similar to that identified originally by Humphries and Vincent (1978), and elaborated later by Sato, Vincent, and Pui (1996) in their studies of particle transport in the recirculating flows in the wakes of simple-shaped bluff bodies.

The structure of the *vena contracta* is also influenced by α. At large sampling velocities or small R ($R = 0.38$ in this case), the size of the *vena contracta* has to be considerably large. When this happens, the influence of orientation would be minimal compared to the effect of the *vena contracta* itself. This is evident from Figure 4a. When $R > 1$, there is flow reversal inside the sampling tube since the stagnation point now shifts from inside the tube when $R < 1$ to outside when $R > 1$. It is evident from the above discussion on the results that *vena contracta* and flow reversal effects produce losses over different ranges of St at a given orientation. Figure 7 is a schematic of the effect of R on the overall sampling efficiency (E_α) at a arbitrary orientation. At low R values when the sampling velocity is high, *vena contracta* is significant and influences particles with small St. Particles with greater inertia tend to ignore the presence of the *vena contracta* as a result of which the sampling efficiency tends to increase slightly before the effects of impaction and gravitational settling becomes significant.

In Figure 7, when $R > 1$, flow reversal inside the sampling inlet will tend to produce effects similar to the *vena contracta*—causing more particles with small St to be deposited while larger particles tend to ignore this flow reversal. The regions of St where *vena contracta* effects and flow reversal are dominant are obviously different. As R increases further, the effect of flow reversal is so significant that the occurrence of a maximum, found so dominant for $R = 1.52$ now almost disappears. Instead, the sampling efficiency falls sharply followed by a rise to a small maximum before impaction and gravitational settling pulls the sampling efficiency curve further down. At best, this is only a qualitative description of a very complex phenomenon. Hence, an empirical expression was developed to model penetration efficiency.

In general, further discussion requires more knowledge of the nature of the *vena contracta* and flow reversal than is available

at present, including how it changes with the angle of the tube and the roles of turbulent-like fluctuating motions and overall stability (i.e., vortex shedding).

CONCLUDING REMARKS

A study has been carried out to explore the nature of particle deposition losses close to the entry of a thin-walled aerosol sampling tube placed at an angle to the wind. Three different loss mechanisms have been proposed: direct impaction on to inner walls geometrically exposed to the upstream flow, and gravitational settling and inertial losses for particles entering the *vena contracta* recirculating flow region located just inside the tube entry. Together, these produce a complex effect on the overall entry losses.

The findings of this research have a significant bearing on how the theory of aerosol sampling may be related to practical applications, both in the development and testing of new sampling devices and in interpreting the results of existing ones. It has been customary to assume that aspiration is the primary index by which to define the particle size-selective performances of aerosol sampling devices. However, this work indicates clearly that the losses of particles immediately post-aspiration is a significant factor in determining overall performance.

REFERENCES

Belyaev, S. P., and Levin, L. M. (1974). Techniques for collection of representative aerosol samples, *J. Aerosol Sci.* 5:325–338.

Davies, C. N., and Subari, M. (1982). Aspiration above wind velocity of aerosols with thin-walled nozzles facing and at right angles to the wind direction, *J. Aerosol Sci.* 13:59–71.

Durham, M. D., and Lundgren, D. A. (1980). Evaluation of aerosol aspiration efficiency as a function of Stokes' number, velocity ratio and nozzle angle, *J. Aerosol Sci.* 11:179–188.

Grinshpun, S., Willeke, K., and Kalatoor, S. (1993). A general equation for aerosol aspiration by thin-walled sampling probes from calm and moving air, *Atmos. Environ.* 27A:1459–1470.

Hangal, S., and Willeke, K. (1990). Overall efficiency of tubular inlets sampling at 0–90 degrees from horizontal air flows, *Atmos. Environ.* 24A:2379–2386.

Humphries, W., and Vincent, J. H. (1978). The transport of airborne dusts in the near wakes of bluff bodies, *Chem. Eng. Sci.* 33:1141–1146.

Jayasekera, P. N., and Davies, C. N. (1980). Aspiration below wind velocity of aerosols with sharp-edged nozzles facing the wind, *J. Aerosol Sci.* 11:535–47.

Okazaki, K., Wiener, R. W., and Willeke, K. (1987a). The combined effect of aspiration and transmission on aerosol sampling accuracy for horizontal isoaxial sampling, *Atmos. Environ.* 21:1181–1185.

Okazaki, K., Wiener, R. W., and Willeke, K. (1987b). Isoaxial sampling: Nondimensional representation of overall sampling efficiency, *Envi. Sci. Tech.* 21:178–182.

Okazaki, K., Wiener, R. W., and Willeke, K. (1987c). Nonisoaxial aerosol sampling: Mechanisms controlling the overall sampling efficiency, *Envi. Sci. Tech.* 21:183–187.

Okazaki, K., and Willeke, K. (1987). Transmission and deposition behavior of aerosols in sampling inlets, *Aerosol Sci. Tech.* 7:275–283.

Ramachandran, G., Sreenath, A., and Vincent J. H. (1998). Towards a new method for experimental determination of aerosol sampler aspiration efficiency in small wind tunnels, *J. Aerosol Sci.* 29:875–891.

Sato S. Vincent, J. H., and Pui, D. Y. H. (1996). Dispersion of large particles in the near wake of a disc in a turbulent freestream. *J. Aerosol. Sci.* 27:559–573.

Tufto, P. A., and Willeke, K. (1982a). Dependence of particulate sampling efficiency on inlet orientation and flow velocities, *Am. Ind. Hyg. Ass. J.* 43:436–443.

Tufto, P. A., and Willeke, K. (1982b). Dynamic evaluation of aerosol sampling inlets, *Envi. Sci. Tech.* 16:607–609.

Vincent, J. H. (1987). Recent advances in aspiration theory for thin-walled and blunt aerosol sampling probes, *J. Aerosol Sci.* 18:487–498.

Vincent, J. H. (1989). *Aerosol Sampling: Science and Practice*. Wiley, London.

Vincent, J. H. (1995). *Aerosol Science for Industrial Hygienists*, Pergamon/Elsevier, Oxford.

Vincent, J. H., Stevens, D. C., Mark, D., Marshall, M., and Smith, T. A. (1986). On the aspiration characteristics of large-diameter, thin-walled aerosol sampling probes at yaw orientation with respect to the wind, *J. Aerosol Sci.* 17:211–224.

Wiener, R. W., Okazaki, K., and Willeke, K. (1988). Influence of turbulence on aerosol sampling efficiency, *Atmos. Environ.* 22:917–928.